

# Explicit Rational Formulae for Bachelier (Normal) Implied Volatility

Fabien Le Floc’h 

Independent researcher; fabien@2ipi.com

## Abstract

We present two explicit rational formulae for Bachelier, or normal, implied volatility. The formulae take the option price, forward, strike, and expiry as inputs and return the implied normal volatility without iteration. They follow the branch structure of LFK-4, but use the simpler near-the-money variable given by the absolute forward-strike difference divided by the tail time value, avoiding a logarithm and a small-argument Taylor branch in that region. LFK-2026 is the accuracy-oriented formula and approximates reciprocal absolute standardized moneyness directly in the far tail. LFK-2026C keeps the same shifted out-of-the-money rational tail approximation, but splits the near-the-money branch into a very small low- $u$  rational and a mid-range rational. In double precision tests both remain close to machine accuracy, while LFK-2026C is the faster scalar implementation on the current benchmark mix.

**Keywords:** Bachelier model; normal implied volatility; bp vol; implied volatility; rational approximation; computational finance

---

## 1. Introduction

The Bachelier model, introduced in Bachelier’s 1900 thesis [1], is widely used when prices are naturally described by a normal volatility rather than a lognormal volatility. Its call price is explicit once the volatility is known, but the inverse problem—recovering the normal volatility from an observed option price—has no elementary closed form. A root finder is robust, but it is often too expensive for calibration, risk, and large grid calculations where the inverse must be evaluated millions of times.

This is not only a numerical issue. In interest-rate derivatives, normal or Bachelier volatilities are the usual convention when forwards, strikes, or rates can be close to zero or negative. Empirical work on low-rate swaption markets therefore considers Black, Bachelier, and shifted-lognormal volatility quotes across currencies including EUR, USD, GBP, and JPY [10]; in particular, the convention has long been familiar in Japanese-yen interest-rate markets. The same modelling issue briefly appeared outside rates in April 2020, when WTI crude oil futures traded below zero. CME Clearing then announced a switch of its options pricing and valuation model to Bachelier to accommodate negative underlying futures prices and negative strikes [4]; Choi, Kwak, Tee, and Wang [2] review this temporary commodity-exchange transition from Black–Scholes to Bachelier.

In interest-rate markets the same implied quantity is often quoted as *basis-point volatility*, or bp vol. This is not a separate volatility model: it is the normal, equivalently Bachelier, volatility expressed in the natural absolute units of the underlying. For a rate forward quoted as a decimal, a normal volatility  $\sigma$  corresponds to  $10^4\sigma$  basis points per square-root year. This contrasts with Black or lognormal volatility, which is dimensionless and measures proportional rather than absolute moves.

We use the standard option terminology throughout: at the money (ATM) means  $F = K$ ; for a call, in the money (ITM) means  $F > K$ , and out of the money (OTM) means  $F < K$ . The formulae are written with the OTM time value, so the same expressions also cover the reflected ITM side through put–call symmetry.

Explicit approximations fill this gap. The LFK-4 approximation [9] is a standard reference: it transforms the inverse problem into a small number of rational approximations, using one branch near the money and

three branches in the OTM tail. Related work includes the direct arithmetic Brownian-motion implied-volatility approximation of Choi, Kim, and Kwak [3]. That work is useful as a compact closed-form reference, but it is not aimed at the near-machine-epsilon accuracy sought by LFK-4 and by LFK-2026 here. For context, Jäckel's rational inversion of the Black–Scholes formula [7] shows the same high-accuracy philosophy in a different model; his normal implied-volatility approximation is also a popular production reference. QuantLib [11] includes an implementation in this family, but it is not a fully faithful transcription of Jäckel's original code and is less accurate. The timings below therefore compare the local Java implementations used in this study rather than the QuantLib port. The goal here is to keep the practical LFK-4 structure while improving the accuracy–cost trade-off. The two formulae below are designed to be portable: they use only arithmetic operations and a logarithm in the OTM routing variable. Both LFK-2026 and LFK-2026C avoid the final OTM square root by fitting  $1/|d|$  directly.

Accurate validation of these formulae requires an accurate forward Bachelier price. Direct formulas for the OTM time value suffer cancellation in the tails, which can make an inverse approximation look worse than it is. For benchmarking we therefore compute the OTM time value with a symmetric erfcx expression; this makes the comparison primarily about the inverse formula rather than about loss of precision in the price used as input.

## 2. Setup and Notation

Let

$$x = F - K, \quad v = \sigma\sqrt{T}, \quad d = \frac{x}{v}.$$

The undiscounted Bachelier call price is

$$C = x\Phi(d) + v\phi(d).$$

Thus ATM corresponds to  $m = |x| = 0$ . Away from ATM, the call is ITM for  $x > 0$  and OTM for  $x < 0$ ; the reflected put side gives the same time value. As in LFK-4, the inverse is expressed in terms of the out-of-the-money time value and the absolute moneyness,

$$c_{\text{otm}} = \begin{cases} C - x, & x > 0, \\ C, & x \leq 0, \end{cases} \quad m = |x|.$$

At the money, where  $m = 0$ , the inverse is exact:

$$\sigma = \frac{C\sqrt{2\pi}}{\sqrt{T}}.$$

For  $m > 0$ , define

$$g = \frac{c_{\text{otm}}}{m}, \quad \alpha = 0.15, \quad \beta_s = -\ln \alpha, \quad \beta_e = 300 \ln(10).$$

The ITM/near-ATM branch is used when  $g > \alpha$ . The OTM branch uses

$$\tilde{\eta} = -\frac{\ln g + \beta_s}{\beta_e - \beta_s}.$$

The three OTM zones are

| $j$ | $\tilde{\eta}$ range |
|-----|----------------------|
| 1   | $[0, 0.011)$         |
| 2   | $[0.011, 0.105)$     |
| 3   | $[0.105, 1]$ .       |

For all coefficient tables, rational functions are written in ascending powers:

$$R_{p,q}(y; a, b) = \frac{P_p(y)}{Q_q(y)}, \quad P_p(y) = \sum_{i=0}^p a_i y^i, \quad Q_q(y) = \sum_{i=0}^q b_i y^i, \quad b_0 = 1.$$

For numerical evaluation, the same polynomials may be evaluated by ordinary Horner steps in descending powers.

### 3. Reference: LFK-4

LFK-4 [9] uses

$$z = \frac{m}{m + c_{\text{otm}}}, \quad \eta = \frac{-z}{\ln(1 - z)}.$$

For small  $z$ , the original algorithm evaluates  $\eta$  by a Taylor expansion; otherwise it uses  $\log 1p(-z)$ . This avoids cancellation in the near-ATM limit. For  $g > \alpha$ , LFK-4 returns

$$\sigma = \frac{m + c_{\text{otm}}}{\sqrt{T}} h_{\text{LFK}}(\eta),$$

with a P7/Q5 rational. For  $g \leq \alpha$ , it fits  $d^2$  with three P9/Q7 rationals in  $\tilde{\eta}$ , using the zones listed above.

### 4. LFK-2026

LFK-2026 uses the no-log ITM variable

$$u = \frac{z}{1 - z} = \frac{m}{c_{\text{otm}}}.$$

For  $g > \alpha$ , it uses a P10/Q9 rational:

$$\sigma = \frac{m + c_{\text{otm}}}{\sqrt{T}} R_{10,9}(u; a_I^{26}, b_I^{26}).$$

In the OTM branch, LFK-2026 approximates  $1/|d|$  directly:

$$W_j^{26}(\tilde{\eta}) = R_{10,9}(\tilde{\eta}; a_j^{26}, b_j^{26}), \quad \sigma = \frac{m}{\sqrt{T}} W_j^{26}(\tilde{\eta}).$$

This removes the final square root in the OTM branch. The method uses more coefficients in the ITM branch than LFK-2026C, but the two methods share the same OTM rational approximation and the same direct OTM accuracy envelope.

### 5. LFK-2026C

LFK-2026C uses the same no-log ITM variable  $u = m/c_{\text{otm}}$ , but splits the ITM branch at  $u = 0.20$ . For small  $u$  it uses a compact P4/Q4 rational, and otherwise it uses a P9/Q8 rational:

$$\sigma = \frac{m + c_{\text{otm}}}{\sqrt{T}} \begin{cases} R_{4,4}(u; a_L^{26C}, b_L^{26C}), & u < 0.20, \\ R_{9,8}(u; a_I^{26C}, b_I^{26C}), & u \geq 0.20. \end{cases}$$

In the OTM branch it uses the same shifted-zone  $1/|d|$  approximation as LFK-2026:

$$W_j^{26C}(\tilde{\eta}) = R_{10,9}(\tilde{\eta}; a_j^{26}, b_j^{26}), \quad \sigma = \frac{m}{\sqrt{T}} W_j^{26C}(\tilde{\eta}).$$

This is the fast variant. It keeps the OTM accuracy of LFK-2026 while reducing the average cost of the ITM/near-ATM branch.

## 6. Numerical Results

### 6.1. Implementations of the Bachelier Formula

A naive implementation of the Bachelier formula, used in many production systems consists in using the standard routines for the cumulative normal distribution and normal probability density function. This leads to somewhat large errors in the prices of very out-of-the-money options. A nice way to look at it is to first compute the prices considering a fixed volatility  $\sigma = 1$ , time-to-maturity  $T = 1$ , varying  $|d|$ , and to invert the resulting option price back using a bisection method to maximum accuracy. In the bisection method, the reference price is given by a multiple precision arithmetic implementation of the Bachelier formula.

In Figure 1, we sample 100,000 uniformly distributed values  $|d| \in [0, 35]$  and compute the maximum relative error in ULP (Unit in the Last Place) for the Bachelier implied volatility in 100 uniform buckets. This clearly shows the loss of accuracy in the very out-of-the-money region for the naive implementation.

A better idea presented in [9] is to use a symmetric  $\operatorname{erfcx}$  expression for the OTM time value. With  $a = m/v$ ,

$$c_{\text{otm}} = e^{-a^2/2} \left( \frac{v}{\sqrt{2\pi}} - \frac{m}{2} \operatorname{erfcx} \left( \frac{a}{\sqrt{2}} \right) \right),$$

which avoids cancellation in both deep ITM and deep OTM cases. There are different implementations of the  $\operatorname{erfcx}$  function, we show the default Julia SpecialFunctions.jl implementation, based on Steven G. Johnson Faddeeva package, and the more accurate implementation found in the Java Apache Commons Numbers library. It is closer to the money ( $|d| \leq 5$ ) that the latter results in a (small) improvement in accuracy. Cody [5] also provides an accurate representation of  $\operatorname{erfcx}$ , and its most accurate pieces are reused in Apache Commons Numbers.

Peter Jäckel [7] gives an even more accurate implementation of the Bachelier formula. Inspired by Cody's  $\operatorname{erfcx}$  formula, he derives a rational function representation of

$$\tilde{\Phi}(u) = \Phi(u) + \frac{\phi(u)}{u},$$

for  $u \in \mathbb{R}$ . This is then used to compute the option price through  $C = x\tilde{\Phi}(d)$ . Except very close to the money, the ULP error in implied volatility is essentially zero, which is remarkable.

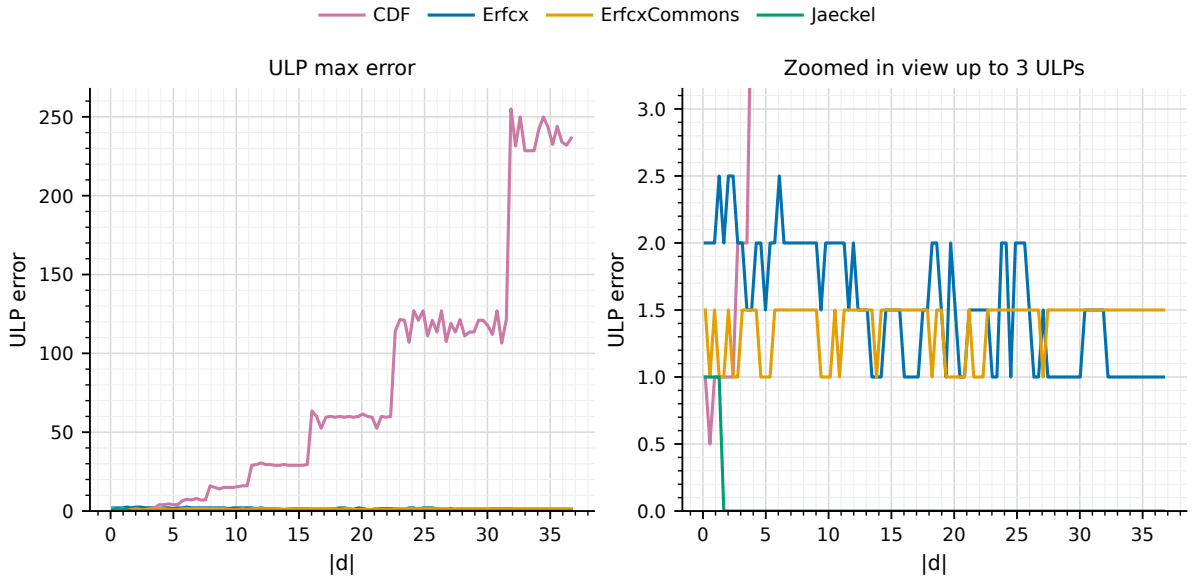


**Figure 1.** Error in the volatility implied from different Bachelier option price implementations.

Noticing that the naive Bachelier formula is very accurate for  $|d| < d_j$ , with  $d_j = 0.61200318096248076056$  being the first cutoff of  $\tilde{\Phi}$  implementation, we may combine Jäckel's representation for  $|d| > d_j$  with the naive Bachelier formula for  $|d| \leq d_j$ . This has the dual benefit of being slightly more accurate (although we

may really wonder if it makes sense to care so much about errors below 1 ULP) and using the classic naive implementation for  $|d|$  values which correspond to typical real market prices. We will however consider the Jäckel formula to compute reference prices in 64-bit floating point numbers, unless otherwise stated.

## 6.2. Accuracy of the Rational Formulae for the Bachelier Implied Volatility

We start by reproducing the example of Le Floc’h [9] of options of maturity  $T = 1$  with forward  $F = 1.0$  and volatility  $\sigma = 1.0$  with varying strikes in Table 1. However, this kind of test can be misleading as there are not enough strikes sampled to hit the worst case scenario of a given approximation. We added a strike at 2.7838494978971955 to show a worst case for LFK-4.

**Table 1.** Error in the Bachelier volatility implied from Jäckel Bachelier price implementation for  $\sigma = 1.0$ ,  $T = 1.0$ ,  $F = 1.0$ .

| Strike   | LFK-4    | LFK-2026 | LFK-2026C | Jaeckel2017 |
|----------|----------|----------|-----------|-------------|
| 1.000010 | 4.44e-16 | 2.22e-16 | 1.11e-16  | 0           |
| 1.006660 | 0        | 2.22e-16 | 2.22e-16  | 0           |
| 2.000000 | 2.22e-16 | 0        | 0         | 0           |
| 2.783849 | 1.33e-15 | 0        | 0         | 0           |
| 4.000000 | 4.44e-16 | 0        | 0         | 0           |
| 8.800000 | 0        | 2.22e-16 | 2.22e-16  | 0           |
| 9.000000 | 0        | 4.44e-16 | 4.44e-16  | 0           |
| 30.00000 | 2.22e-16 | 4.44e-16 | 4.44e-16  | 0           |

It is a better idea to randomly sample from a space of parameters that covers the whole region of interest for the argument  $d = (F - K)/(\sigma\sqrt{T})$ . We do this in Table 2, where we sample 40,000,000 uniform values in several buckets for  $|d| \in [0, 35]$  and compute the maximum relative error in ULP for the Bachelier implied volatility.

**Table 2.** Absolute volatility error statistics per bucket and overall

| Bucket                                   | Approximation | Cases       | Max      | Worst $d$          | $p_{95}$ | $p_{99}$ |
|------------------------------------------|---------------|-------------|----------|--------------------|----------|----------|
| <b>Bucket 0.00 — range [0.00, 1.00]</b>  |               |             |          |                    |          |          |
| 0.00                                     | LFK-4         | 40,000,000  | 1.33e-15 | 0.5306090208459261 | 4.44e-16 | 6.66e-16 |
| 0.00                                     | LFK-2026      | 40,000,000  | 1.22e-15 | 0.7783018038945502 | 4.44e-16 | 4.44e-16 |
| 0.00                                     | LFK-2026C     | 40,000,000  | 9.99e-16 | 0.7700211092071692 | 3.33e-16 | 4.44e-16 |
| 0.00                                     | Jaeckel2017   | 40,000,000  | 5.55e-16 | 0.6121702394114410 | 2.22e-16 | 2.22e-16 |
| <b>Bucket 1.00 — range [1.00, 2.00]</b>  |               |             |          |                    |          |          |
| 1.00                                     | LFK-4         | 40,000,000  | 1.33e-15 | 1.7896497885619913 | 8.88e-16 | 9.99e-16 |
| 1.00                                     | LFK-2026      | 40,000,000  | 8.88e-16 | 1.9791769043189662 | 3.33e-16 | 4.44e-16 |
| 1.00                                     | LFK-2026C     | 40,000,000  | 8.88e-16 | 1.9791769043189662 | 3.33e-16 | 4.44e-16 |
| 1.00                                     | Jaeckel2017   | 40,000,000  | 4.44e-16 | 1.1742267194679015 | 2.22e-16 | 2.22e-16 |
| <b>Bucket 2.00 — range [2.00, 32.00]</b> |               |             |          |                    |          |          |
| 2.00                                     | LFK-4         | 40,000,000  | 1.55e-15 | 2.6491128666595603 | 6.66e-16 | 8.88e-16 |
| 2.00                                     | LFK-2026      | 40,000,000  | 1.22e-15 | 4.1572426607873700 | 4.44e-16 | 6.66e-16 |
| 2.00                                     | LFK-2026C     | 40,000,000  | 1.22e-15 | 4.1572426607873700 | 4.44e-16 | 6.66e-16 |
| 2.00                                     | Jaeckel2017   | 40,000,000  | 2.22e-16 | 3.0937788117606120 | 0.00e+00 | 2.22e-16 |
| <b>Overall (all buckets combined)</b>    |               |             |          |                    |          |          |
| –                                        | LFK-4         | 158,816,168 | 1.55e-15 | 2.649113           | 6.66e-16 | 8.88e-16 |
| –                                        | LFK-2026      | 158,816,168 | 1.22e-15 | 0.778302           | 4.44e-16 | 4.44e-16 |
| –                                        | LFK-2026C     | 158,816,168 | 1.22e-15 | 4.157243           | 4.44e-16 | 4.44e-16 |
| –                                        | Jaeckel2017   | 160,000,000 | 5.55e-16 | 0.612170           | 2.22e-16 | 2.22e-16 |

## 7. Pushing Accuracy Further

When we look at the error in multiple precision arithmetic, we notice that the new variants LFK-2026 and LFK-2026C are more accurate than LFK-4 (Figure 2). We also derived an even more accurate approximation in multiple precision arithmetic called LFK-2026D (we give the coefficients in Appendix J). As shown in Table 2,

this does not lead to improved accuracy in 64-bit floating-point arithmetic when using a straightforward Horner-method implementation (Algorithm 1) for evaluating the rational functions. The classic implementation of

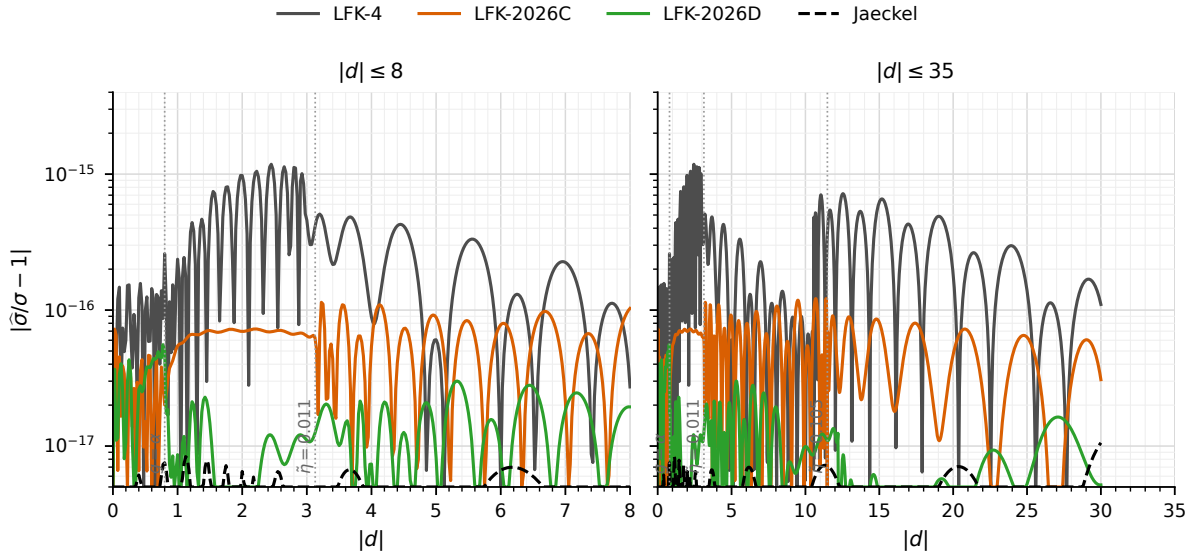


**Figure 2.** Direct BigFloat relative implied-volatility error for LFK-4, LFK-2026, and LFK-2026C. The left panel focuses on the central region  $|d| \leq 8$ , while the right panel shows the full direct grid  $|d| \leq 35$ . The dotted vertical lines mark the route boundary  $g = \alpha$  and the two OTM zone boundaries.

**Input:**  $x \in \mathbb{R}$ , coefficients  $c = (c_0, c_1, \dots, c_{n-1})$   
**Output:**  $y = c_0 + c_1x + c_2x^2 + \dots + c_{n-1}x^{n-1}$

```

1  $y \leftarrow c_0$ ;
2 for  $i \leftarrow 1$  to  $n - 1$  do
3    $y \leftarrow y \cdot x + c_i$ ;
4 end
5 return  $y$ ;

```

**Algorithm 1:** Classic Horner scheme for polynomial evaluation

Horner's method is suboptimal in terms of floating point error. One slight improvement consists in using fused-multiply-add (FMA) instructions in the Horner evaluation. Another advantage of FMA is improved speed (at least on x86 architectures) as shown in Algorithm 2.

**Input:**  $x \in \mathbb{R}$ , coefficients  $c = (c_0, c_1, \dots, c_{n-1})$   
**Output:**  $y = \sum_{i=0}^{n-1} c_i x^i$  evaluated with FMA for each step

```

1  $y \leftarrow c_0$ ;
2 for  $i \leftarrow 1$  to  $n - 1$  do
3    $y \leftarrow \text{fma}(y, x, c_i)$ ;
4 end
5 return  $y$ ;

```

**Algorithm 2:** Horner scheme with fused multiply-add (FMA)

If the ultimate goal is to increase accuracy even closer to machine epsilon, one solution is to use the compensated Horner FMA scheme, where the error is accumulated and added back to the main approximation [8]:

The FMA implementation (suffix + in Table 3) is slightly more accurate (by around 2 machine epsilons), and the compensated horner (suffix ++) let LFK-2026++ and LFK-2026C++ reach an maximum error of 3 machine epsilons (6.66e-16). The LFK-2026D++ is not more accurate in float64 arithmetic despite being more accurate in multiple-precision arithmetic.

|                                                                                               |                                                         |
|-----------------------------------------------------------------------------------------------|---------------------------------------------------------|
| <b>Input:</b> $x \in \mathbb{R}$ , coefficients $c = (c_0, c_1, \dots, c_{n-1})$              |                                                         |
| <b>Output:</b> $y = \sum_{i=0}^{n-1} c_i x^i$ evaluated with compensated arithmetic using FMA |                                                         |
| 1                                                                                             | $s \leftarrow c_0;$                                     |
| 2                                                                                             | $e \leftarrow 0;$                                       |
| 3                                                                                             | <b>for</b> $i \leftarrow 1$ <b>to</b> $n - 1$ <b>do</b> |
| 4                                                                                             | $p \leftarrow s \cdot x;$                               |
| 5                                                                                             | $pe \leftarrow \text{fma}(s, x, -p);$                   |
| 6                                                                                             | $t \leftarrow p + c_i;$                                 |
| 7                                                                                             | $z \leftarrow t - p;$                                   |
| 8                                                                                             | $te \leftarrow (p - (t - z)) + (c_i - z);$              |
| 9                                                                                             | $s \leftarrow t;$                                       |
| 10                                                                                            | $e \leftarrow \text{fma}(e, x, pe + te);$               |
| 11                                                                                            | <b>end</b>                                              |
| 12                                                                                            | <b>return</b> $s + e;$                                  |

**Algorithm 3:** Compensated Horner scheme with FMA

**Table 3.** Absolute volatility error statistics per bucket and overall for LFK-2026 variants. The suffix + denotes FMA implementation and ++ denotes the compensated Horner FMA scheme.

| Bucket                                   | Approximation | Cases       | Max      | Worst $d$           | $p_{95}$ | $p_{99}$ |
|------------------------------------------|---------------|-------------|----------|---------------------|----------|----------|
| <b>Bucket 0.00 — range [0.00, 1.00]</b>  |               |             |          |                     |          |          |
| 0.00                                     | LFK-2026+     | 40,000,000  | 8.88e-16 | 0.7631171052449106  | 2.22e-16 | 4.44e-16 |
| 0.00                                     | LFK-2026++    | 40,000,000  | 6.66e-16 | 0.7749365794558335  | 2.22e-16 | 2.22e-16 |
| 0.00                                     | LFK-2026C+    | 40,000,000  | 8.88e-16 | 0.7582758869622748  | 2.22e-16 | 4.44e-16 |
| 0.00                                     | LFK-2026C++   | 40,000,000  | 5.55e-16 | 0.9830956928512565  | 2.22e-16 | 2.22e-16 |
| 0.00                                     | LFK-2026D+    | 40,000,000  | 9.99e-16 | 0.7280022477431374  | 2.22e-16 | 4.44e-16 |
| 0.00                                     | LFK-2026D++   | 40,000,000  | 6.66e-16 | 0.7675775666172642  | 2.22e-16 | 2.22e-16 |
| <b>Bucket 1.00 — range [1.00, 2.00]</b>  |               |             |          |                     |          |          |
| 1.00                                     | LFK-2026+     | 40,000,000  | 6.66e-16 | 1.8237757808060500  | 2.22e-16 | 3.33e-16 |
| 1.00                                     | LFK-2026++    | 40,000,000  | 5.55e-16 | 1.0475809080916290  | 2.22e-16 | 2.22e-16 |
| 1.00                                     | LFK-2026C+    | 40,000,000  | 6.66e-16 | 1.8237757808060500  | 2.22e-16 | 3.33e-16 |
| 1.00                                     | LFK-2026C++   | 40,000,000  | 5.55e-16 | 1.0475809080916290  | 2.22e-16 | 2.22e-16 |
| 1.00                                     | LFK-2026D+    | 40,000,000  | 6.66e-16 | 1.7722558130136150  | 2.22e-16 | 4.44e-16 |
| 1.00                                     | LFK-2026D++   | 40,000,000  | 4.44e-16 | 1.7803130699297630  | 2.22e-16 | 2.22e-16 |
| <b>Bucket 2.00 — range [2.00, 32.00]</b> |               |             |          |                     |          |          |
| 2.00                                     | LFK-2026+     | 40,000,000  | 1.11e-15 | 9.4045676549501300  | 4.44e-16 | 4.44e-16 |
| 2.00                                     | LFK-2026++    | 40,000,000  | 6.66e-16 | 7.9895611392130190  | 2.22e-16 | 2.22e-16 |
| 2.00                                     | LFK-2026C+    | 40,000,000  | 1.11e-15 | 9.4045676549501300  | 4.44e-16 | 4.44e-16 |
| 2.00                                     | LFK-2026C++   | 40,000,000  | 6.66e-16 | 7.9895611392130190  | 2.22e-16 | 2.22e-16 |
| 2.00                                     | LFK-2026D+    | 40,000,000  | 8.88e-16 | 27.3829069373139650 | 3.33e-16 | 4.44e-16 |
| 2.00                                     | LFK-2026D++   | 40,000,000  | 4.44e-16 | 7.8976758999678350  | 2.22e-16 | 2.22e-16 |
| <b>Overall (all buckets combined)</b>    |               |             |          |                     |          |          |
| –                                        | LFK-2026+     | 158,816,168 | 1.11e-15 | 9.404568            | 3.33e-16 | 4.44e-16 |
| –                                        | LFK-2026++    | 158,816,168 | 6.66e-16 | 0.774937            | 2.22e-16 | 2.22e-16 |
| –                                        | LFK-2026C+    | 158,816,168 | 1.11e-15 | 9.404568            | 3.33e-16 | 4.44e-16 |
| –                                        | LFK-2026C++   | 158,816,168 | 6.66e-16 | 7.989561            | 2.22e-16 | 2.22e-16 |
| –                                        | LFK-2026D+    | 158,816,168 | 9.99e-16 | 0.728002            | 2.22e-16 | 4.44e-16 |
| –                                        | LFK-2026D++   | 158,816,168 | 6.66e-16 | 0.767578            | 2.22e-16 | 2.22e-16 |

In Figure 3, we sample the space of normalized OTM Bachelier distances  $|d|$  in the range  $0 \leq |d| \leq 35$ , uniformly. For each input, the target volatility is 1.0, while each implementation returns a 64-bit floating point approximation  $y = \text{float64}(\text{approximation}(x))$ . The ULP error is then computed as

$$\text{ulp}(x) = \frac{|y - y_{\text{ref}}|}{\text{ulp}(y_{\text{ref}})},$$

where  $\text{ulp}(y_{\text{ref}}) = |\text{nextfloat}(y_{\text{ref}}) - y_{\text{ref}}|$  is the distance between adjacent 64-bit floating-point numbers at  $y_{\text{ref}}$ . This normalizes the absolute error into units of machine epsilon, so that  $\text{ulp} = 1$  corresponds to an error of one floating-point step. The  $|d|$  range is split into 1000 equal-width bins, and for each bin we record the maximum and RMS ULP error over  $10^6$  random samples. This removes call-price rounding and intrinsic-subtraction effects, so the plot shows the rational-approximation ULP error itself.

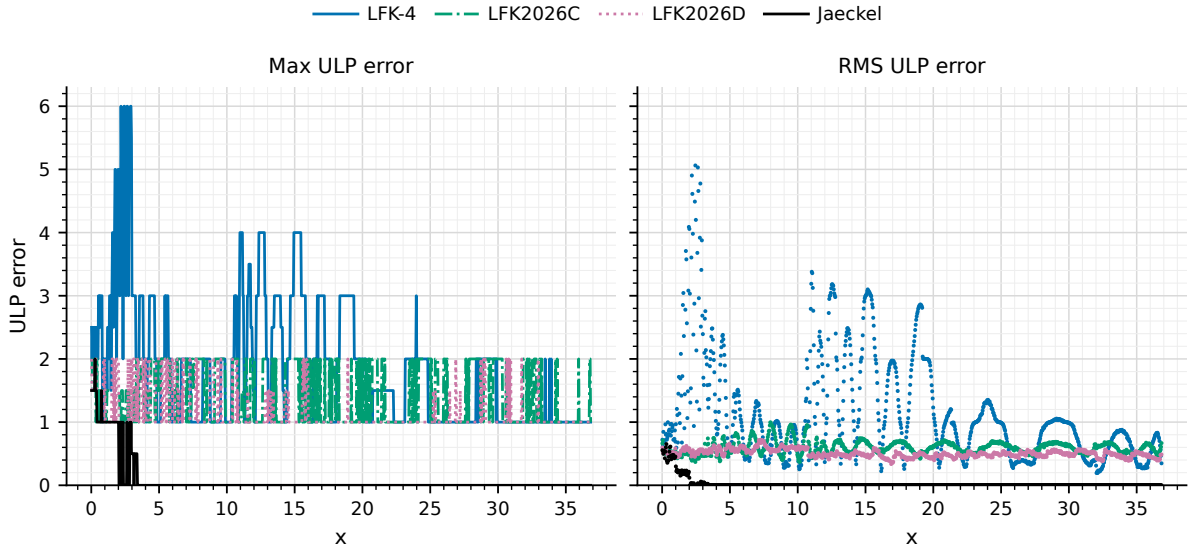


**Figure 3.** Relative implied-volatility error in ULP. LFK-2026C and LFK-2026D use the compensated Horner FMA scheme.

As a final test, we consider the example from Cui et al. [6], which consists of a three-dimensional data set of size  $40 \times 40 \times 40$  with forward  $F = 1.0$ . Discrete points of  $K$  are uniformly generated from 1.01 to 10,  $\sigma$  from 0.01 to 0.99, and  $T$  from 0.01 to 2. Samples with option prices less than  $10^{-20}$  are filtered out, leaving 29 330 retained samples.

In Table 4, we report a much higher accuracy for Jäckel algorithm than the authors. The discrepancy is likely the choice of implementation for the Bachelier option price. We use the highly accurate Jäckel Bachelier option price implementation, while they likely use the naive CDF implementation. The LFK-2026+ is nearly

**Table 4.** Absolute volatility error statistics and timing for the 3D grid experiment (Cui et al.)

| Method      | AbsErrorMean | AbsErrorDev | AbsErrorMax | AbsErrorMin | Time(sec) |
|-------------|--------------|-------------|-------------|-------------|-----------|
| LFK-2026+   | 1.00e-16     | 9.87e-17    | 6.66e-16    | 0           | 2.30e-08  |
| LFK-2026++  | 7.42e-17     | 7.88e-17    | 5.55e-16    | 0           | 5.13e-08  |
| LFK-2026C+  | 9.97e-17     | 9.87e-17    | 6.66e-16    | 0           | 2.34e-08  |
| LFK-2026C++ | 7.40e-17     | 7.89e-17    | 5.55e-16    | 0           | 5.04e-08  |
| LFK-2026D+  | 9.22e-17     | 9.25e-17    | 6.66e-16    | 0           | 2.47e-08  |
| LFK-2026D++ | 6.88e-17     | 7.50e-17    | 4.44e-16    | 0           | 5.11e-08  |
| Jäckel-2017 | 3.96e-17     | 5.53e-17    | 3.33e-16    | 0           | 6.58e-08  |

three times faster than Jäckel-2017 and gives up very little in accuracy. LFK-2026D++ is slightly more accurate than the other LFK-2026 formulas on this example, this is consistent with the lower RMSE observed in Figure 3.



### 7.1. Timing

The timing table below uses a rotated-order scalar benchmark and reports medians over fifty rounds. This is more stable than the fixed-order main report, whose single sequential timing slices can move when CPU frequency or scheduling changes during the run. Absolute timings are machine- and power-state-dependent; the relative ordering is the more reproducible part of the table.

**Table 5.** Timing results on an Intel(R) Core(TM) Ultra 5 245KF CPU running Java 25.0.3 for implying the volatility of options of strikes  $K \in \{1.001, 1.01, 1.1, 1.5, 2.0, 3.0, 5.0, 7.0, 8.0, 0.999, 0.99, 0.9, 0.5, 0.0, -0.5, -1.0\}$  and forward  $F = 1$ , volatility  $\sigma = 1$ , maturity  $T = 1$ .

| Approximation | median ns/call | Relative to LFK-4 |
|---------------|----------------|-------------------|
| LFK-4         | 12.36          | 1.00              |
| LFK-2026      | 9.51           | 0.77              |
| LFK-2026+     | 7.85           | 0.64              |
| LFK-2026++    | 22.41          | 1.81              |
| LFK-2026C     | 9.41           | 0.76              |
| LFK-2026C+    | 7.77           | 0.63              |
| LFK-2026C++   | 20.50          | 1.66              |
| Jäckel        | 25.75          | 2.08              |

## Appendix H LFK-2026 Coefficients

### Appendix H.1 ITM/near-ATM branch

| $i$ | $a_{i,i}^{26}$           | $b_{i,i}^{26}$          |
|-----|--------------------------|-------------------------|
| 0   | 2.50662827463100069e+00  | 1.0000000000000000e+00  |
| 1   | 8.26914966237441540e+00  | 3.79891342328838499e+00 |
| 2   | 1.10083895644891214e+01  | 5.87074621959482457e+00 |
| 3   | 7.62695942399991100e+00  | 4.76157470081986212e+00 |
| 4   | 2.96457253391146036e+00  | 2.18581925252758946e+00 |
| 5   | 6.51812439800918964e-01  | 5.72905243689549204e-01 |
| 6   | 7.81257091685455263e-02  | 8.27294623127229206e-02 |
| 7   | 4.67776338554095131e-03  | 6.05262799121958784e-03 |
| 8   | 1.17427118047196583e-04  | 1.90358881940080979e-04 |
| 9   | 8.06959950534549627e-07  | 1.76070970713414280e-06 |
| 10  | -3.39451638335349906e-10 |                         |

### Appendix H.2 OTM branch, zone 1

| $i$ | $a_{1,i}^{26}$           | $b_{1,i}^{26}$          |
|-----|--------------------------|-------------------------|
| 0   | 1.24910559446641112e+00  | 1.0000000000000000e+00  |
| 1   | 8.30013684602045146e+02  | 9.50178311644246946e+02 |
| 2   | 2.89118707775471907e+05  | 4.30671117130989209e+05 |
| 3   | 6.20616261157058701e+07  | 1.19319078802154481e+08 |
| 4   | 8.81948242946073532e+09  | 2.18139815883858109e+10 |
| 5   | 8.14953597568851318e+11  | 2.66113331187980811e+12 |
| 6   | 4.61473754119971406e+13  | 2.08194332615256938e+14 |
| 7   | 1.32385751716178975e+15  | 9.31612904921204000e+15 |
| 8   | 1.35683441709766740e+16  | 1.78457095251951296e+17 |
| 9   | 2.23602102096865640e+16  | 9.01018167981477888e+17 |
| 10  | -1.15188057059215700e+16 |                         |

### Appendix H.3 OTM branch, zone 2

| $i$ | $a_{2,i}^{26}$           | $b_{2,i}^{26}$           |
|-----|--------------------------|--------------------------|
| 0   | 1.25087969033276813e+00  | 1.0000000000000000e+00   |
| 1   | 2.09344504116440078e+02  | 4.55619235679538008e+02  |
| 2   | -1.74963499510044603e+04 | 4.19868074702521844e+04  |
| 3   | -1.28046460022976995e+07 | -1.48653150107890852e+07 |
| 4   | -1.43888265763526964e+09 | -4.63359666129231930e+09 |
| 5   | -5.70761754440745773e+10 | -3.39232384615881042e+11 |
| 6   | -8.98414557472468994e+11 | -8.93831987833861328e+12 |
| 7   | -5.46607883881420703e+12 | -9.10822517732905625e+13 |
| 8   | -1.07736581582367109e+13 | -3.32157260465782750e+14 |
| 9   | -3.54669640321780615e+12 | -3.16204789033010312e+14 |
| 10  | 4.53512764886659485e+11  |                          |

### Appendix H.4 OTM branch, zone 3

| $i$ | $a_{3,i}^{26}$           | $b_{3,i}^{26}$          |
|-----|--------------------------|-------------------------|
| 0   | 1.61713874667576762e+00  | 1.0000000000000000e+00  |
| 1   | 1.63839367097254751e+02  | 6.08432004257079598e+02 |
| 2   | 4.52092618390189637e+03  | 3.37041720211591382e+04 |
| 3   | 4.73452995425928821e+04  | 5.83977840443553636e+05 |
| 4   | 2.11536138072810922e+05  | 4.03973802769196732e+06 |
| 5   | 4.14000232322855853e+05  | 1.20766363495907933e+07 |
| 6   | 3.38490556724923430e+05  | 1.55296990844987314e+07 |
| 7   | 9.82243936325080576e+04  | 7.83292053799574263e+06 |
| 8   | 5.74901275345015438e+03  | 1.16810498733679834e+06 |
| 9   | -1.25257952774401772e+02 | 5.54442814599942540e+03 |
| 10  | 4.62144628906322019e+00  |                         |

## Appendix I LFK-2026C Coefficients

### Appendix I.1 Low- $u$ ITM/near-ATM branch, $u < 0.20$

| $i$ | $a_{L,i}^{26C}$         | $b_{L,i}^{26C}$         |
|-----|-------------------------|-------------------------|
| 0   | 2.50662827463100069e+00 | 1.0000000000000000e+00  |
| 1   | 4.33803460770355898e+00 | 2.23062541885758314e+00 |
| 2   | 2.36504153278287266e+00 | 1.63840524330855919e+00 |
| 3   | 4.35189695439266722e-01 | 4.35646805136993498e-01 |
| 4   | 1.77075775698172025e-02 | 2.96543644408861981e-02 |

Appendix I.2 High- $u$  ITM/near-ATM branch,  $u \geq 0.20$

| $i$ | $a_{I,i}^{26C}$          | $b_{I,i}^{26C}$         |
|-----|--------------------------|-------------------------|
| 0   | 2.50662827462874782e+00  | 1.0000000000000000e+00  |
| 1   | 7.07601239545194982e+00  | 3.32292052116718439e+00 |
| 2   | 7.79838748842165330e+00  | 4.35214422048696914e+00 |
| 3   | 4.28317532357895026e+00  | 2.86841498456426436e+00 |
| 4   | 1.24534893861795548e+00  | 1.01064393092251747e+00 |
| 5   | 1.88932466067008031e-01  | 1.87748433761637329e-01 |
| 6   | 1.38619741425921022e-02  | 1.70940757504186268e-02 |
| 7   | 4.15460128562968034e-04  | 6.51089901103861003e-04 |
| 8   | 3.33224453410284549e-06  | 7.12577601891527465e-06 |
| 9   | -1.65051672752885574e-09 |                         |

LFK-2026C uses the same OTM coefficients as LFK-2026 in all three shifted  $\tilde{\eta}$  zones.

## Appendix J LFK-2026D: BigFloat Accuracy Optimised

The three OTM zones of LFK-2026D are

| $j$ | $\tilde{\eta}$ range |
|-----|----------------------|
| 1   | [0, 0.0145)          |
| 2   | [0.0145, 0.1178)     |
| 3   | [0.1178, 1].         |

The coefficients for this LFK-2026D variant are as follows.

Appendix J.1 OTM branch, zone 1

| $i$ | $a_{1,i}^{26}$           | $b_{1,i}^{26}$          |
|-----|--------------------------|-------------------------|
| 0   | 1.24910559446641112e+00  | 1.0000000000000000e+00  |
| 1   | 8.47619772864081597e+02  | 9.64273267539114840e+02 |
| 2   | 2.99702508527653001e+05  | 4.43171035283801029e+05 |
| 3   | 6.53920879898315892e+07  | 1.24538153134200945e+08 |
| 4   | 9.45245193184535408e+09  | 2.31235285898333626e+10 |
| 5   | 8.92378101657744629e+11  | 2.87260538833032178e+12 |
| 6   | 5.19998272533330938e+13  | 2.30100251568817812e+14 |
| 7   | 1.57119179781390850e+15  | 1.06746011913009540e+16 |
| 8   | 1.78880731995660620e+16  | 2.20357803266821088e+17 |
| 9   | 3.63093569588198400e+16  | 1.29402991182225946e+18 |
| 10  | -2.96291760969892680e+16 |                         |

## Appendix J.2 OTM branch, zone 2

| $i$ | $a_{2,i}^{26}$           | $b_{2,i}^{26}$           |
|-----|--------------------------|--------------------------|
| 0   | 1.25070935316808463e+00  | 1.0000000000000000e+00   |
| 1   | 4.91931764982681784e+02  | 6.81403825183943468e+02  |
| 2   | 9.27513975150481565e+04  | 1.95271993660958280e+05  |
| 3   | 7.86397585558160208e+06  | 2.88054137623462491e+07  |
| 4   | 2.88765027905221641e+08  | 1.76543913139240003e+09  |
| 5   | 4.55199642305969429e+09  | 4.49113820497479324e+10  |
| 6   | 2.88783135940116310e+10  | 4.69178670074972595e+11  |
| 7   | 5.89013711536382675e+10  | 1.79968388446012061e+12  |
| 8   | 6.97512731591760159e+09  | 1.60734143390380566e+12  |
| 9   | -1.47094092991961823e+10 | -6.97033196207605225e+11 |
| 10  | 2.83876889443327570e+09  |                          |

## Appendix J.3 OTM branch, zone 3

| $i$ | $a_{3,i}^{26}$           | $b_{3,i}^{26}$          |
|-----|--------------------------|-------------------------|
| 0   | 1.61982027094435455e+00  | 1.0000000000000000e+00  |
| 1   | 1.66989132560739989e+02  | 6.11508302127448815e+02 |
| 2   | 4.77794828200244592e+03  | 3.47884126130892910e+04 |
| 3   | 5.31817138355287098e+04  | 6.32535742841342231e+05 |
| 4   | 2.61260745170476090e+05  | 4.72538757008512411e+06 |
| 5   | 5.91063965520491474e+05  | 1.58891631710913163e+07 |
| 6   | 6.06698667324509122e+05  | 2.44793192915989943e+07 |
| 7   | 2.60718058985714306e+05  | 1.65611815097258985e+07 |
| 8   | 3.82246440507954903e+04  | 4.32860404065594450e+06 |
| 9   | 9.69726676635529088e+02  | 3.10428817652220372e+05 |
| 10  | -9.78571143231221896e+00 |                         |

**Acknowledgments:** This paper would not exist without the initial idea from Gary Kennedy.

**Conflicts of Interest:** The author declares no conflicts of interest.

## References

1. Bachelier, L. Théorie de la spéculation. *Annales Scientifiques de l'École Normale Supérieure* **1900**, *17*, 21–86.
2. Choi, J.; Kwak, M.; Tee, C.W.; Wang, Y. A Black–Scholes User’s Guide to the Bachelier Model. *Journal of Futures Markets* **2022**, *42*, 959–980. <https://doi.org/10.1002/fut.22315>.
3. Choi, J.; Kim, K.; Kwak, M. Numerical Approximation of the Implied Volatility under Arithmetic Brownian Motion. *Applied Mathematical Finance* **2009**, *16*, 261–268.
4. CME Clearing. Switch to Bachelier Options Pricing Model—Effective April 22, 2020. CME Clearing Advisory 20-171, 21 April 2020. Available online: <https://www.cmegroup.com/notices/clearing/2020/04/Chadv20-171.html> (accessed on 18 May 2026).
5. Cody, W. J. Algorithm 715: SPECFUN—a portable FORTRAN package of special function routines and test drivers, *ACM Transactions on Mathematical Software (TOMS)*, **1993**, *19*, 22–30.
6. Cui, Z.; Liu, Y.; Yao, Y. Tighter bounds for implied volatility based on the Dirac delta family method. *Journal of Futures Markets* **2025** <https://doi.org/10.1002/fut>.
7. Jäckel, P. Let’s Be Rational. *Wilmott* **2017**, 40–53. <https://doi.org/10.1002/wilm.10395>.
8. Graillat S., Langlois Ph., Louvet N., Improving the Compensated Horner Scheme with a Fused Multiply and Add. *Research Report RR2005-06, DALI-LP2A Laboratory, Université de Perpignan Via Domitia, November 2005*. Available at: <https://perso.ens-lyon.fr/nicolas.louvet/rr2005-06.pdf>.
9. Le Floc’h, F. Fast and Accurate Analytic Basis Point Volatility. Available online: <https://ssrn.com/abstract=2420757> (accessed on 17 May 2026).

10. Patel, J.; Russo, V.; Fabozzi, F.J. Using the Right Implied Volatility Quotes in Times of Low Interest Rates: An Empirical Analysis across Different Currencies. *Finance Research Letters* **2018**, *25*, 196–201. <https://doi.org/10.1016/j.frl.2017.10.013>.
11. QuantLib Project. QuantLib: A Free/Open-Source Library for Quantitative Finance. Available online: <https://www.quantlib.org/> (accessed on 18 May 2026).